MNRAS **000**, 1–23 (2020) Preprint 21 April 2020 Compiled using MNRAS LATEX style file v3.0

Fine Structure Of Convective-Reactive Zones In Stars

Miroslav Mocák,[1⋆]
[1] *Monash Centre for Astrophysics, School of Physics and Astronomy, Monash University, Clayton, Australia 3800*

in preparation for MNRAS

ABSTRACT
Fine structure of convective-reactive zones in stars ..

Key words: turbulence – convection-reactive events – stellar evolution

1 INTRODUCTION

Based on RANS analysis of composition transport in 3D oxygen burning shell simulation, we find **6 different co-exising convective-reactive structures**. We summarize their properties below.

- quadrupled layer due to H^1 and He^4 (Fig.6,7)
- double layer due to C^{12} (Fig.8)
- double layer due to O^{16}, Ne^{20}, Na^{23}, Si^{28}, Ar^{38}, Ti^{44} (Fig.9,10,11,13,19,23)
- single layer due to Mg^{24}, S^{32}, Ar^{36}, Ca^{40}, Ca^{42} (Fig.12,15,18,21,22)
- tripled layer due to P^{31}, S^{34}, Cl^{35}, K^{39} (Fig.14,16,17,20)
- single neutron burning layer

We also find a single layer of chemical elements, which are not able to burn due to low-temperatures[1], namely Ti^{46}, Cr^{48}, Cr^{50}, Fe^{52}, Fe^{54}, Ni^{56} (Fig.24).

A convective-reactive layer is defined as a region with distinct rate of nuclear burning of a given element balanced by its transport.

Studied properties are derived from three time periods representing the onset of transient period, its end and post-transient period, where the evolution of the 3D model appear quasi-static. Hence, averaging is done around three central times $t_c \sim 460$ s (transient onset), $t_c \sim 760$ s (transient end), $t_c \sim 1060$ s (post-transient) Fig.2. Averaging window is choosen to be 300 seconds (approx. 3 TOs), which is an optimum averaging window giving us robust statistics.

Convective mixing in stars is often not instantaneous, and composition profiles are not flat, but shaped by an interaction of entrainment, transport and nuclear burning of individual chemical elements. It suggests, that modeling of turbulent transport of elements, in burning regions of stars, may need to be done separately for every individual element, until careful analysis shows valid simplications. Here we see that *currents of composition* may connect entrainment regions with burning regions.

⋆ E-mail:miroslav.mocak@gmail.com
[1] i.e. a single transport layer of passive scalars only

2 TRANSPORT EQUATION

Applying RANS averaging rules (Mocák et al. 2014) on the instantaneous evolution equation for mass fraction of element i in spherical geometry,

$$\partial_t\left(\rho X_i\right) = -\nabla\cdot\left(\rho\mathbf{u}X_i\right) + \rho\dot{X}_i^{\mathrm{nuc}} \tag{1}$$

and having additional implicit numerics $\mathcal{N}$ in mind (explained in next paragraphs), we obtain the following 1D transport equation

$$\overline{\rho}\widetilde{D}_t\widetilde{X}_i = -\nabla_r f_i + \overline{\rho}\widetilde{\dot{X}}_i^{\mathrm{nuc}} + \mathcal{N}_i \tag{2}$$

where X_i is mass fraction of chemical element i, ρ is density, $\mathbf{u} = \mathbf{u}(u_r, u_\theta, u_\phi)$ is the velocity vector, ∇ is the divergence operator, $\dot{X}_i^{\mathrm{nuc}}$ is the rate of nuclear burning of i, and $f_i = \overline{\rho}\widetilde{X_i''u_r''}$ is turbulent flux of element i. $\widetilde{D}_t q = \partial_t q + \widetilde{u}_i\partial_i q$ is the mean flow Lagrangian derivative of a variable q and $\nabla_r(.) = (1/r^2)\partial_r r^2(.)$ is the radial divergence operator.

The mean-field transport equation (Eq. 2) tells us that temporal change of mass fraction of an element i in the Lagrangian frame of reference, $\overline{\rho}\widetilde{D}_t\widetilde{X}_i$, is caused either by redistribution due to the turbulent flux f_i by $-\nabla_r f_i$, or by nuclear burning $\overline{\rho}\widetilde{\dot{X}}_i^{\mathrm{nuc}}$. We define the numerical residual in these equations by $\mathcal{N}_i$ and represents the implicit action of our numeric scheme.

3 RELEVANT TIMESCALES

Important features of the simulations are strongly dynamic, and most easily understood in terms of some timescales, which we define here.

The convective turnover timescale is

$$\tau_{\mathrm{conv}} = 2(r_{\mathrm{t}}^c - r_{\mathrm{b}}^c)/v_{\mathrm{rms}}, \tag{3}$$

where r_{b}^c and r_{t}^c are the radii of the bottom and top convection boundaries, and v_{rms} is the rms of the velocity field in the convection zone. The net nuclear (e-folding) burning timescale for element i is

$$\tau_{\mathrm{nucl}}^i = \widetilde{X}_i/\widetilde{\dot{X}}_i^{\mathrm{nuc}} \tag{4}$$

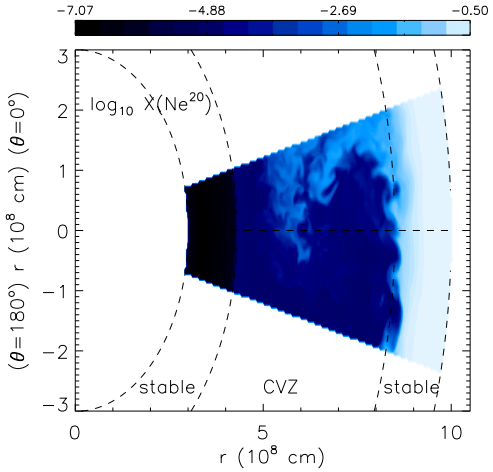

Figure 1. Oxygen burning shell - old graphics, will be replaced

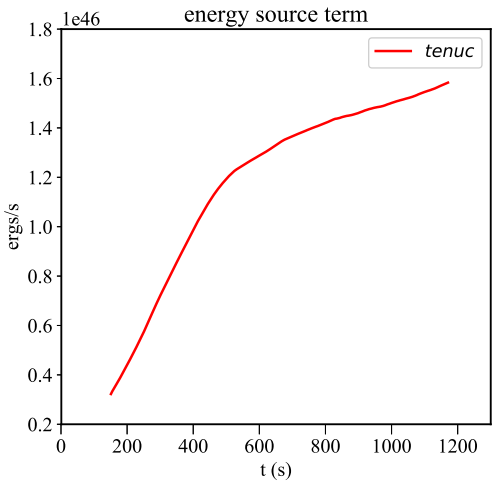

Figure 3. Total nuclear energy production evolution

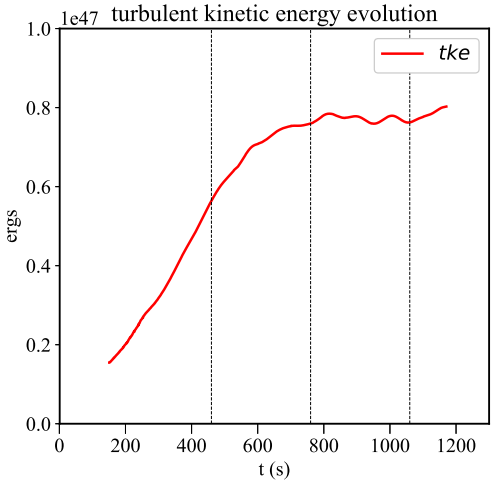

Figure 2. Turbulent kinetic energy evolution, the three vertical lines mark the three central times $t_c \sim 460$ s (transient onset), $t_c \sim 760$ s (transient end), $t_c \sim 1060$ s (post-transient)

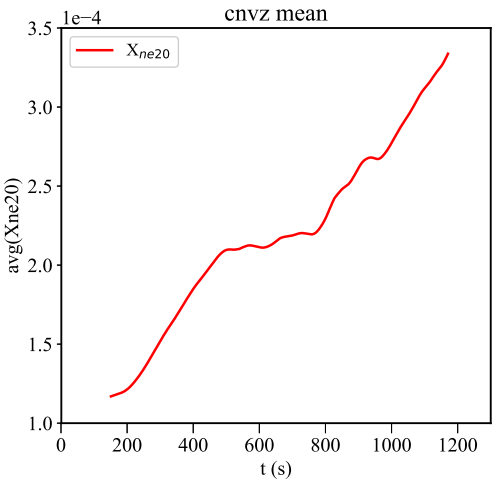

Figure 4. Mean mass fraction of ne20 in convection zone evolution

and the (e-folding) turbulent transport timescale of element i is

$$\tau^i_{\rm tran} = \widetilde{X}_i/(\nabla_r f_i/\overline{\rho}). \quad (5)$$

The (e-folding) background transport timescale of element i is,

$$\tau^i_{\rho \rm X} = \overline{\rho}\widetilde{X}_i/(\partial_t \overline{\rho}\widetilde{X}_i). \quad (6)$$

$$\tau^i_{\rm X} = \widetilde{X}_i/(\partial_t \widetilde{X}_i). \quad (7)$$

4 COMPOSITION STRUCTURE OF CONVECTION ZONE

4.1 Neutrons

4.2 Protons and He^4

4.3 C^{12}, O^{16}, Ne^{20}

4.4 P^{31}, S^{34}, Cl^{35}

4.5 Ar^{38}, K^{39}

4.6 Ni^{56}

HERE PUT ALL THE PASSIVE SC ALARs, elements that don't burn just tranported

AFTER TI44, all looks similar, all are passive scalar, no burning

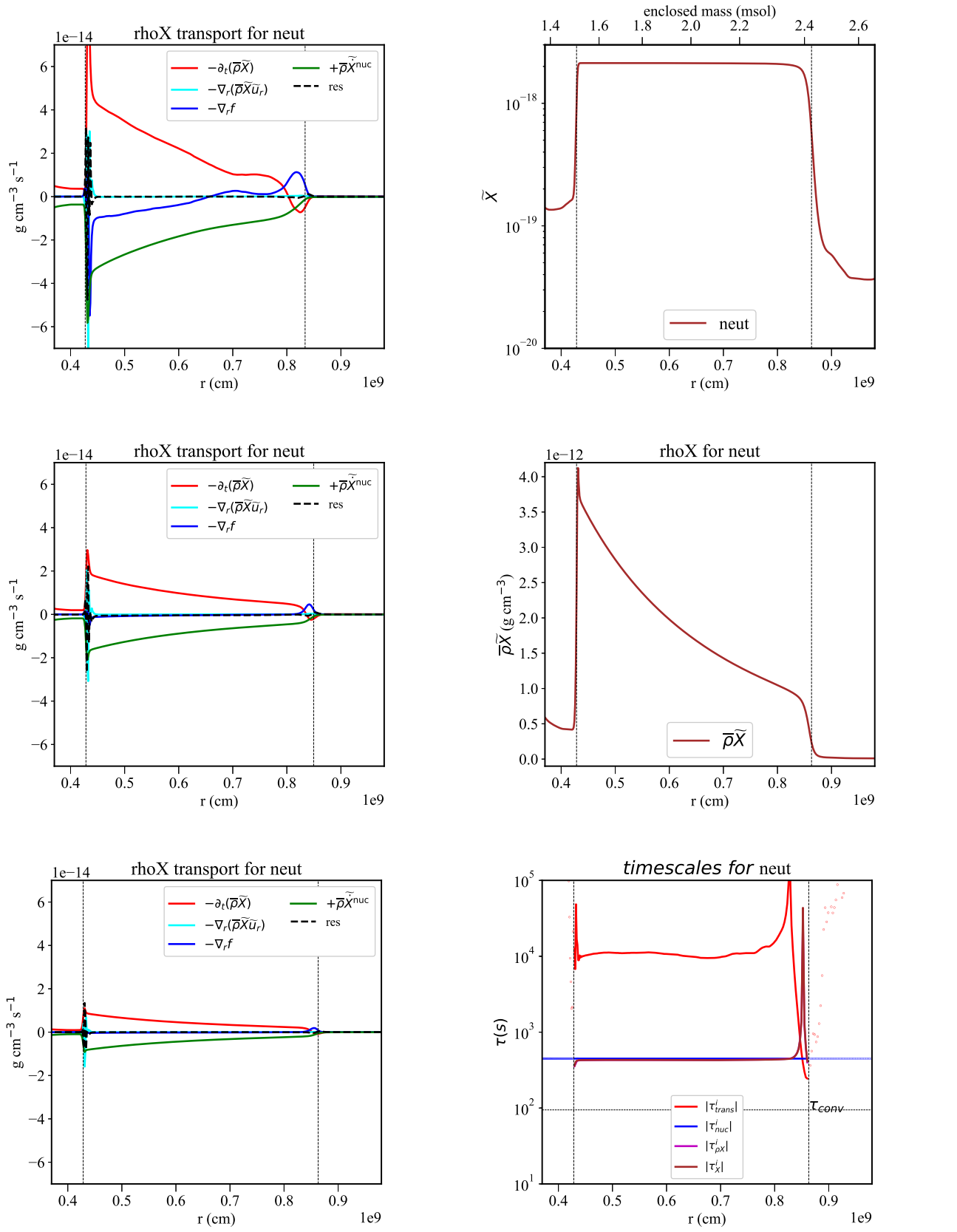

Figure 5. Neutrons: Left (from top to bottom): Transport at $t_c \sim 460$ s, $t_c \sim 760$ s, $t_c \sim 1060$ s. Right (from top to bottom): Mean mass fraction X, mean composition density ρX, various transport timescales at $t_c \sim 1060$ s (see Sect.3).

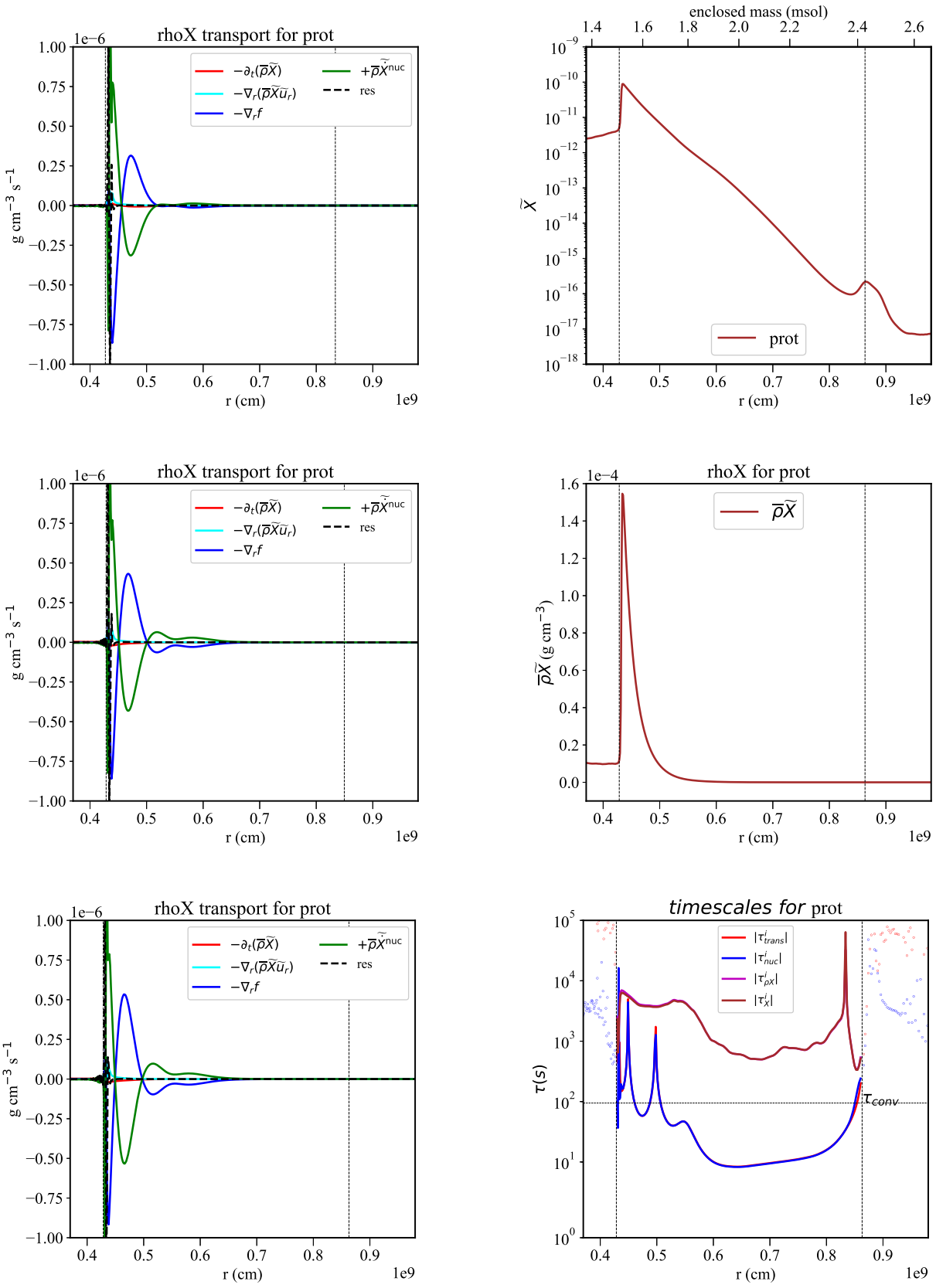

Figure 6. Protons: Plot description defined in Fig.5

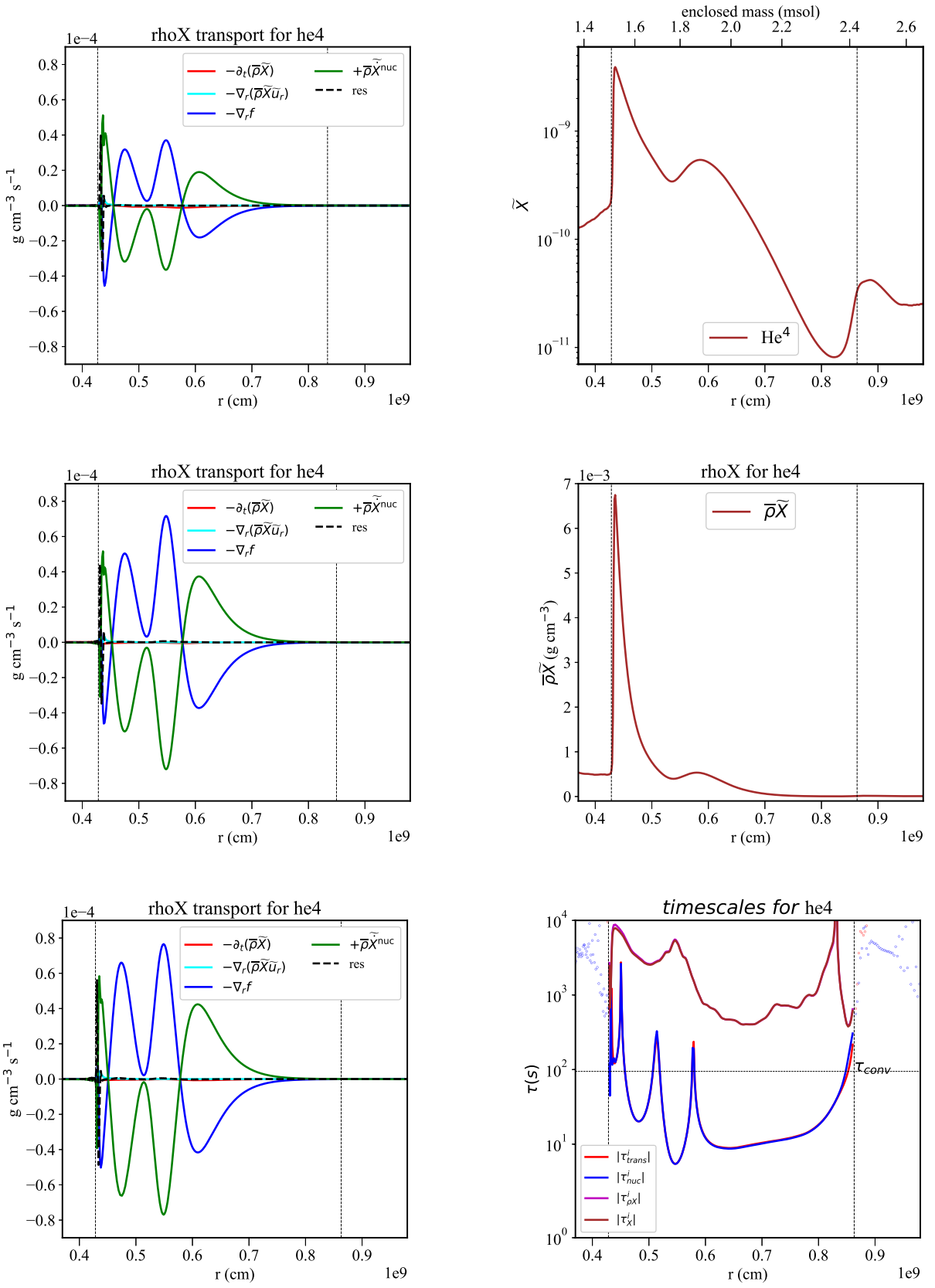

Figure 7. He^4: Plot description defined in Fig.5

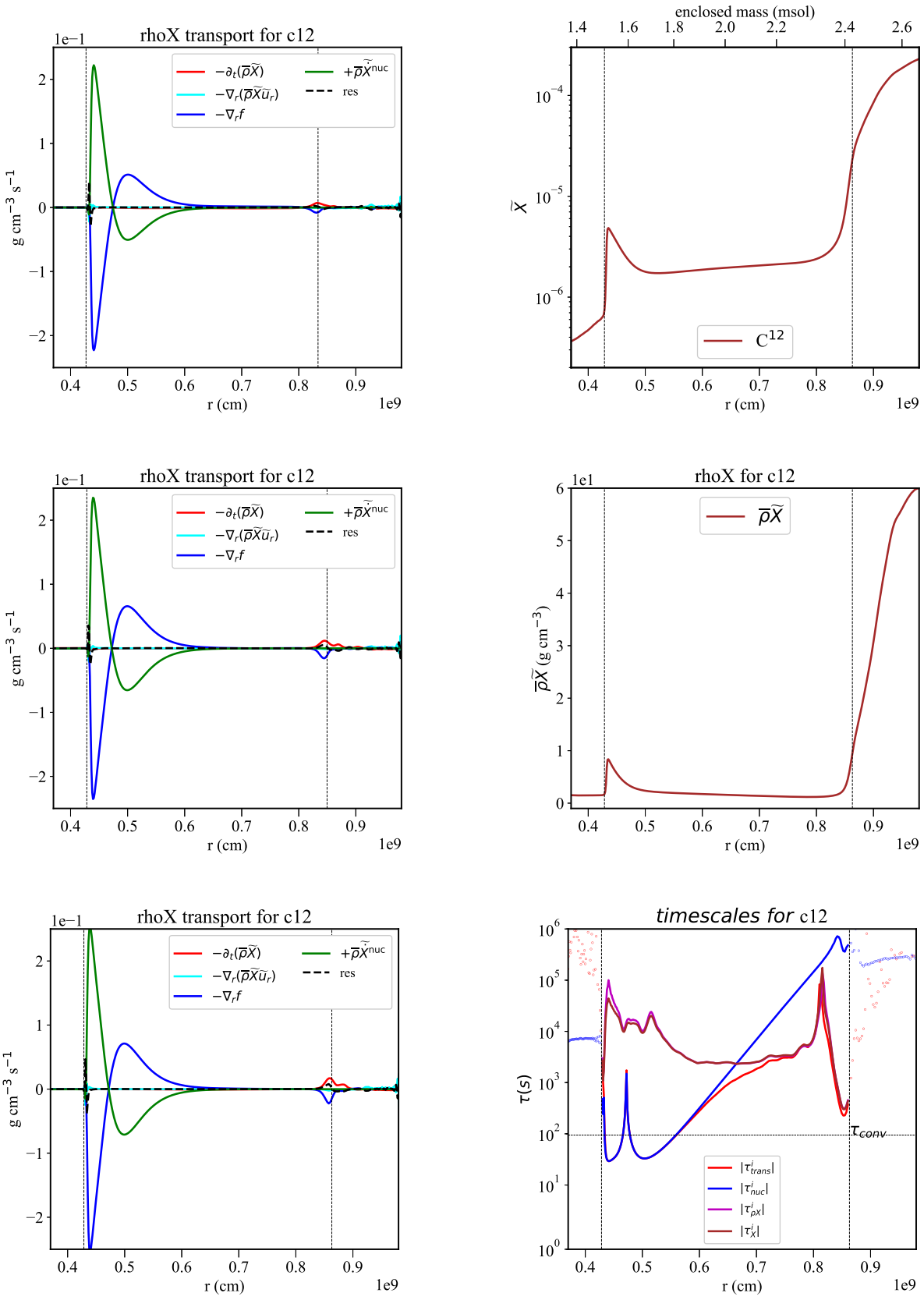

Figure 8. C^{12}: Plot description defined in Fig.5

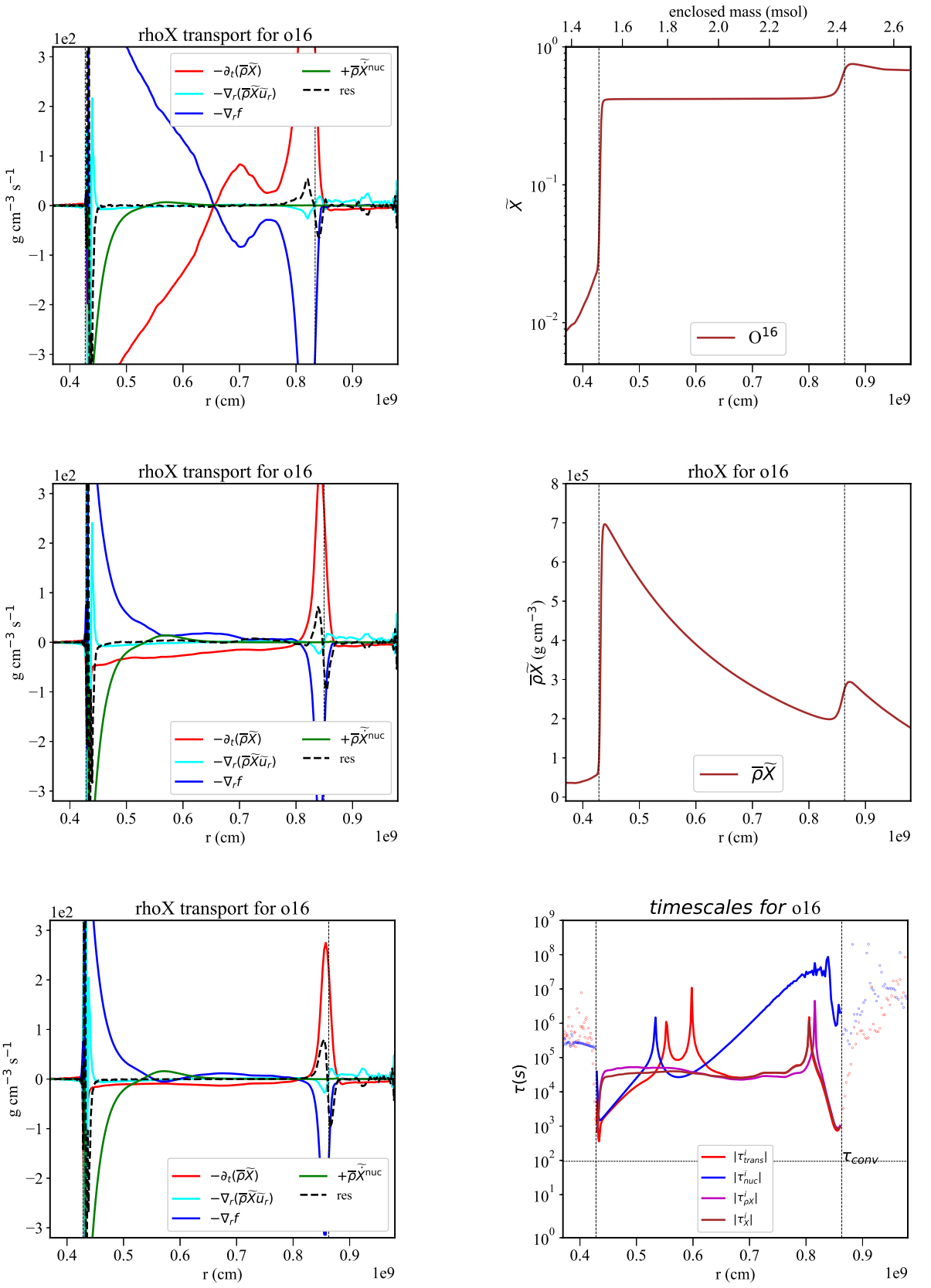

Figure 9. O^{16}: Plot description defined in Fig.5

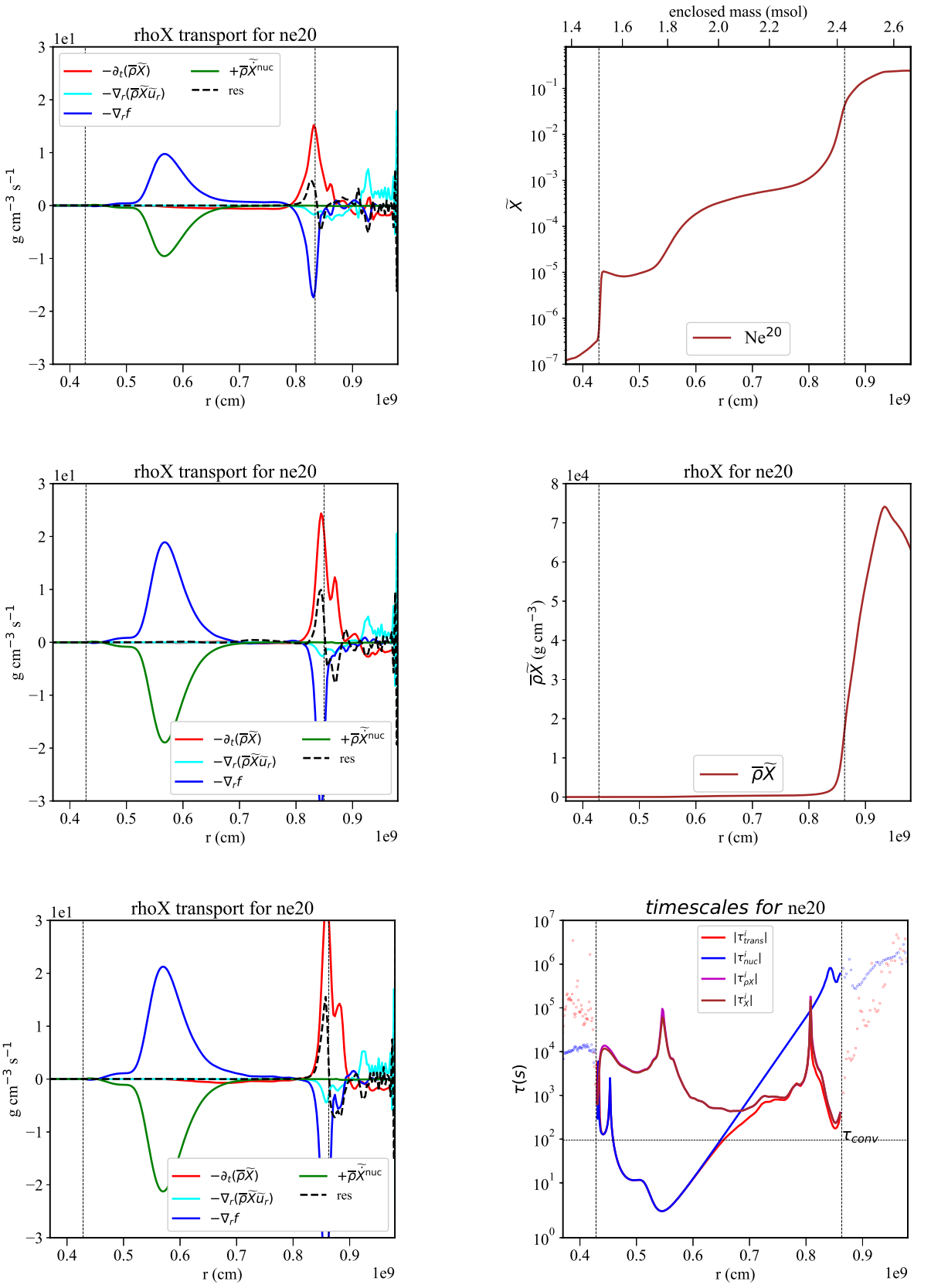

Figure 10. Ne^{20}: Plot description defined in Fig.5

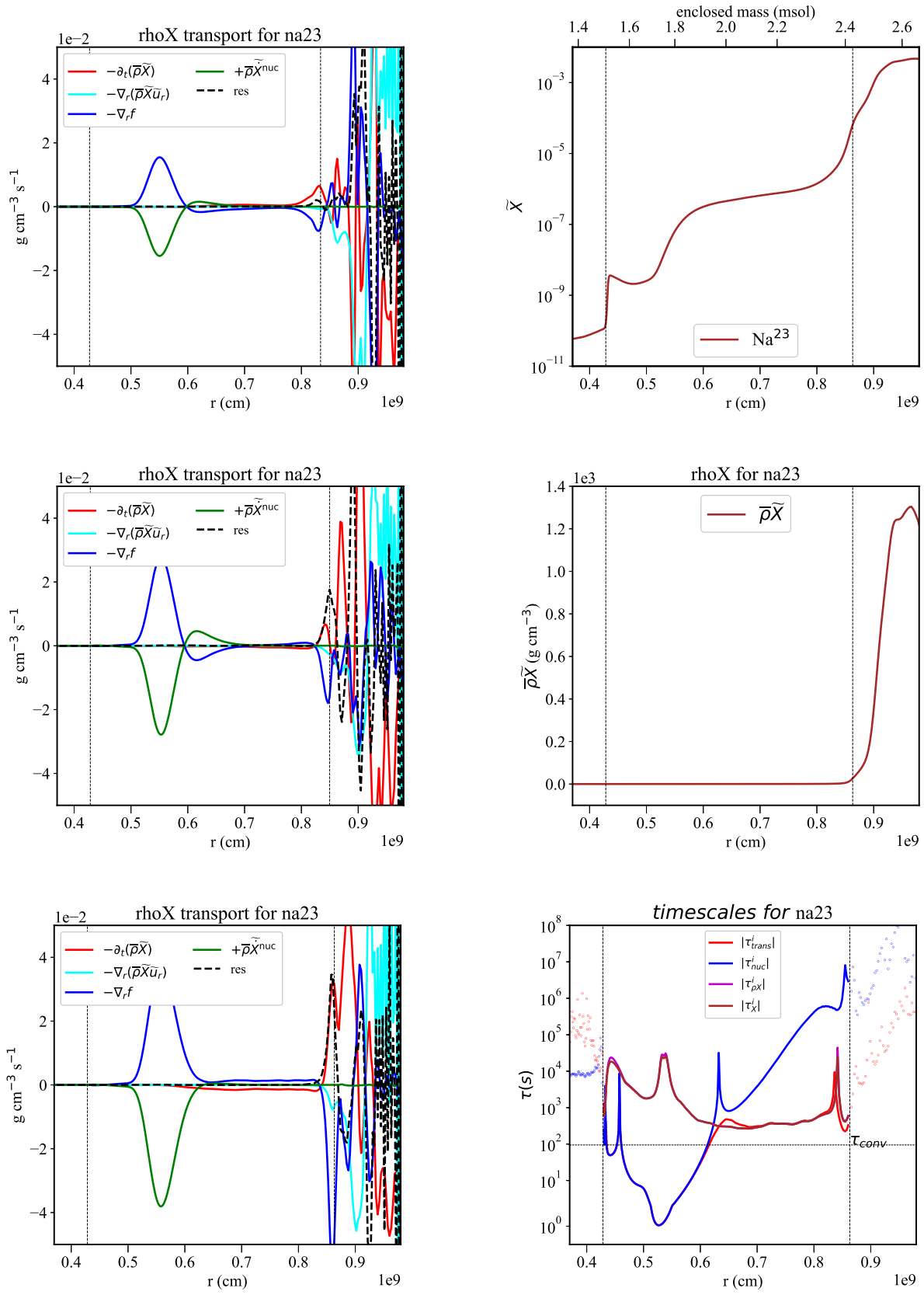

Figure 11. Na^{23}: Plot description defined in Fig.5

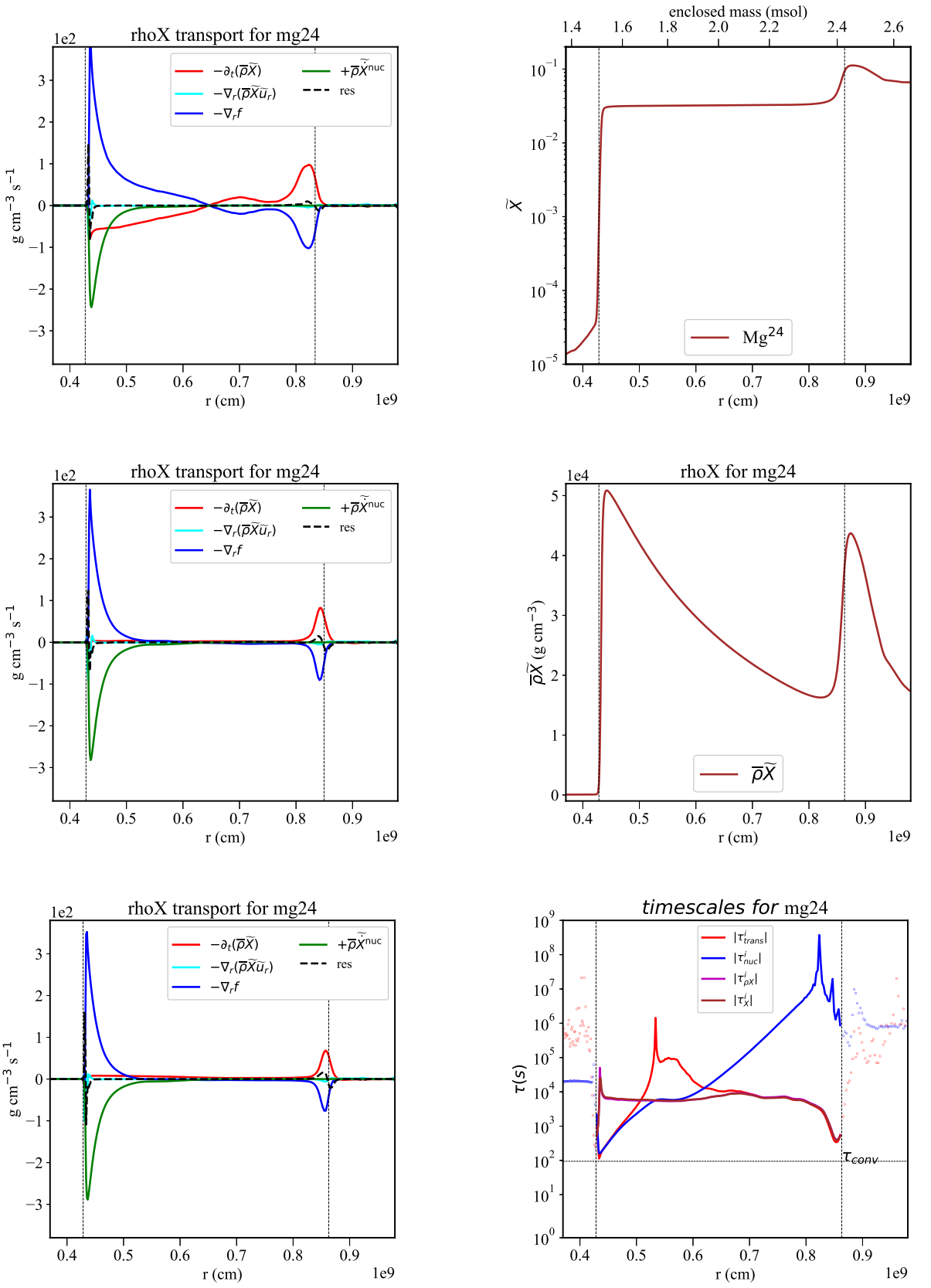

Figure 12. Mg^{24}: Plot description defined in Fig.5

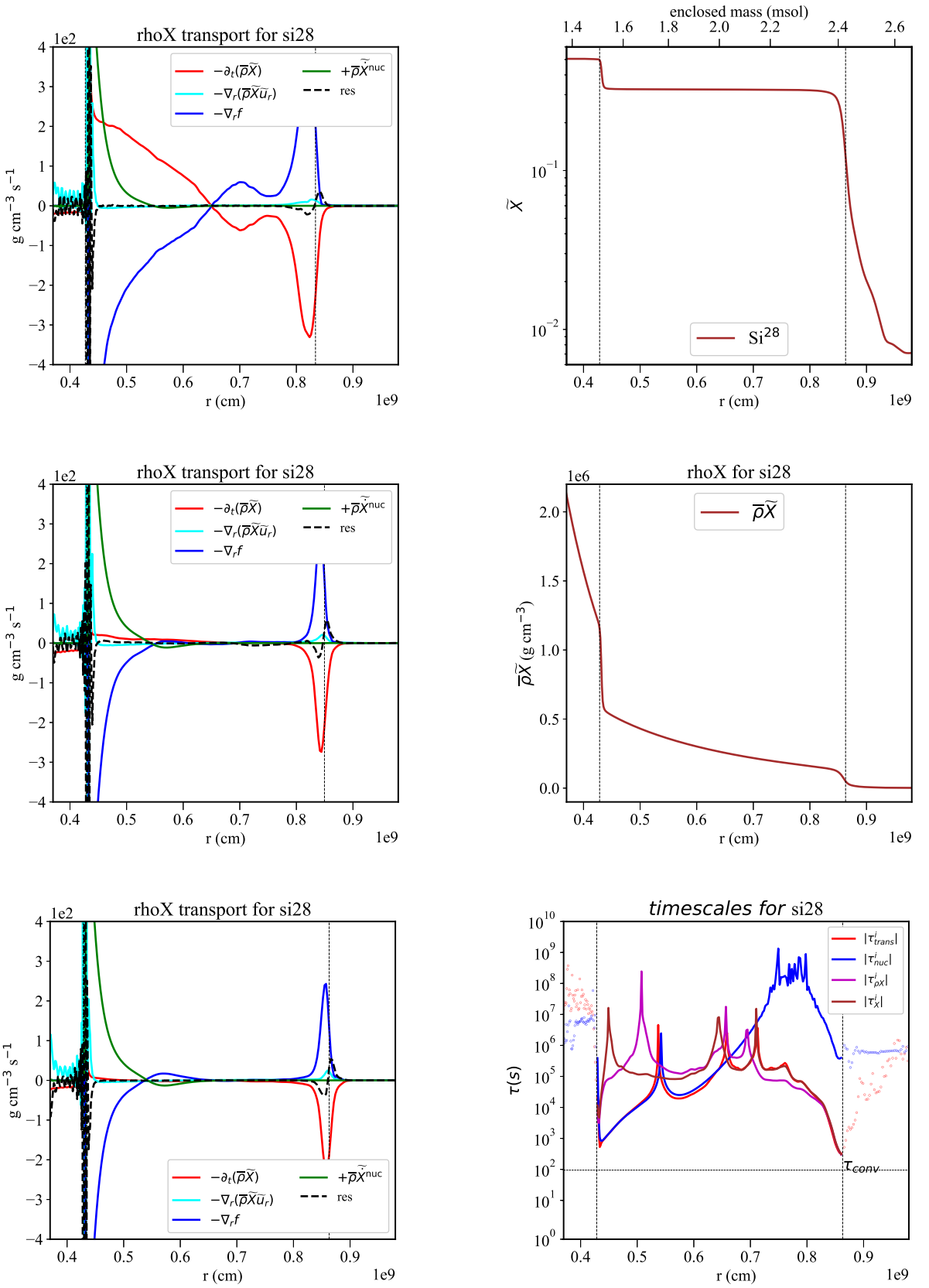

Figure 13. Si^{28}: Plot description defined in Fig.5

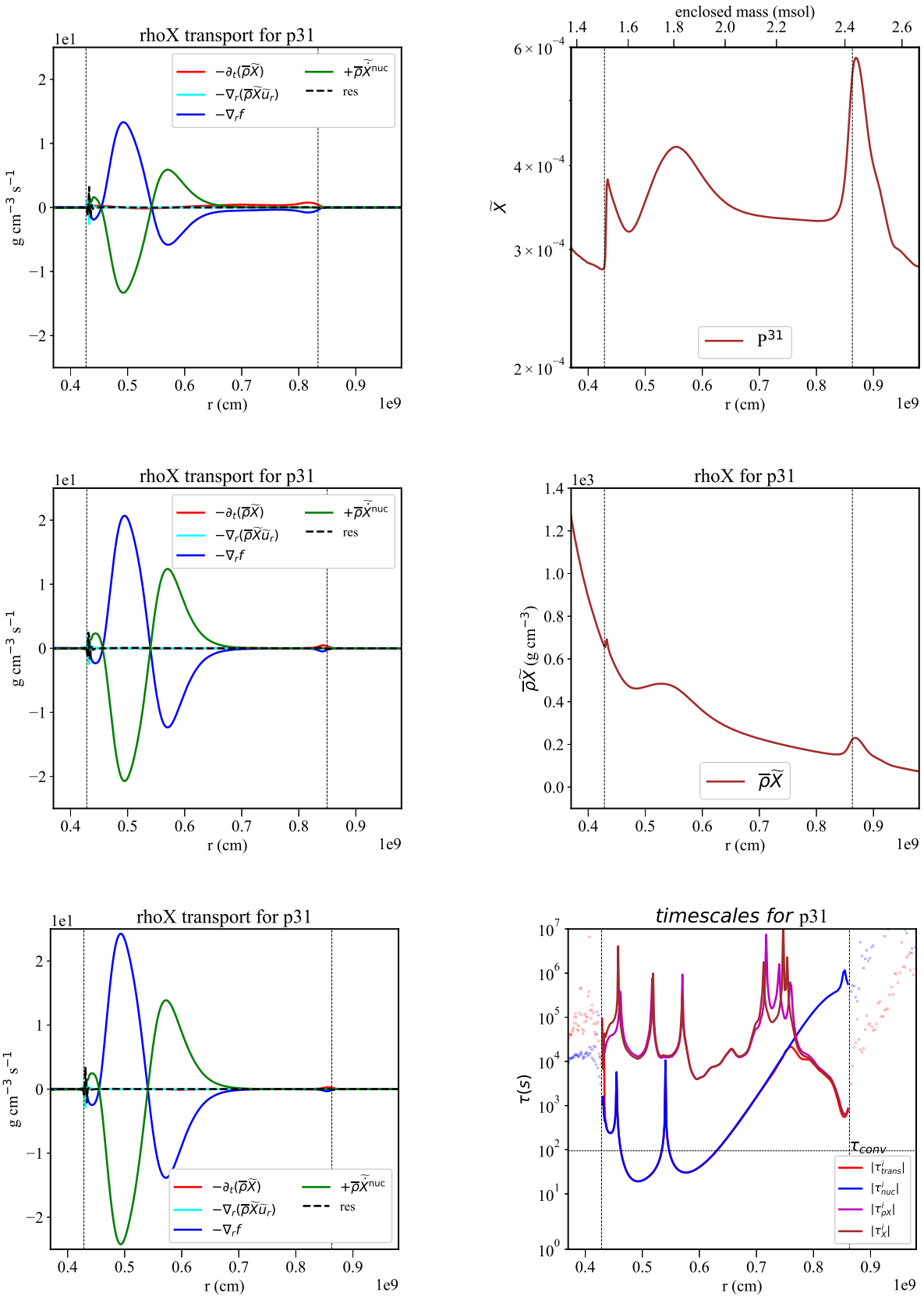

Figure 14. P^{31}: Plot description defined in Fig.5

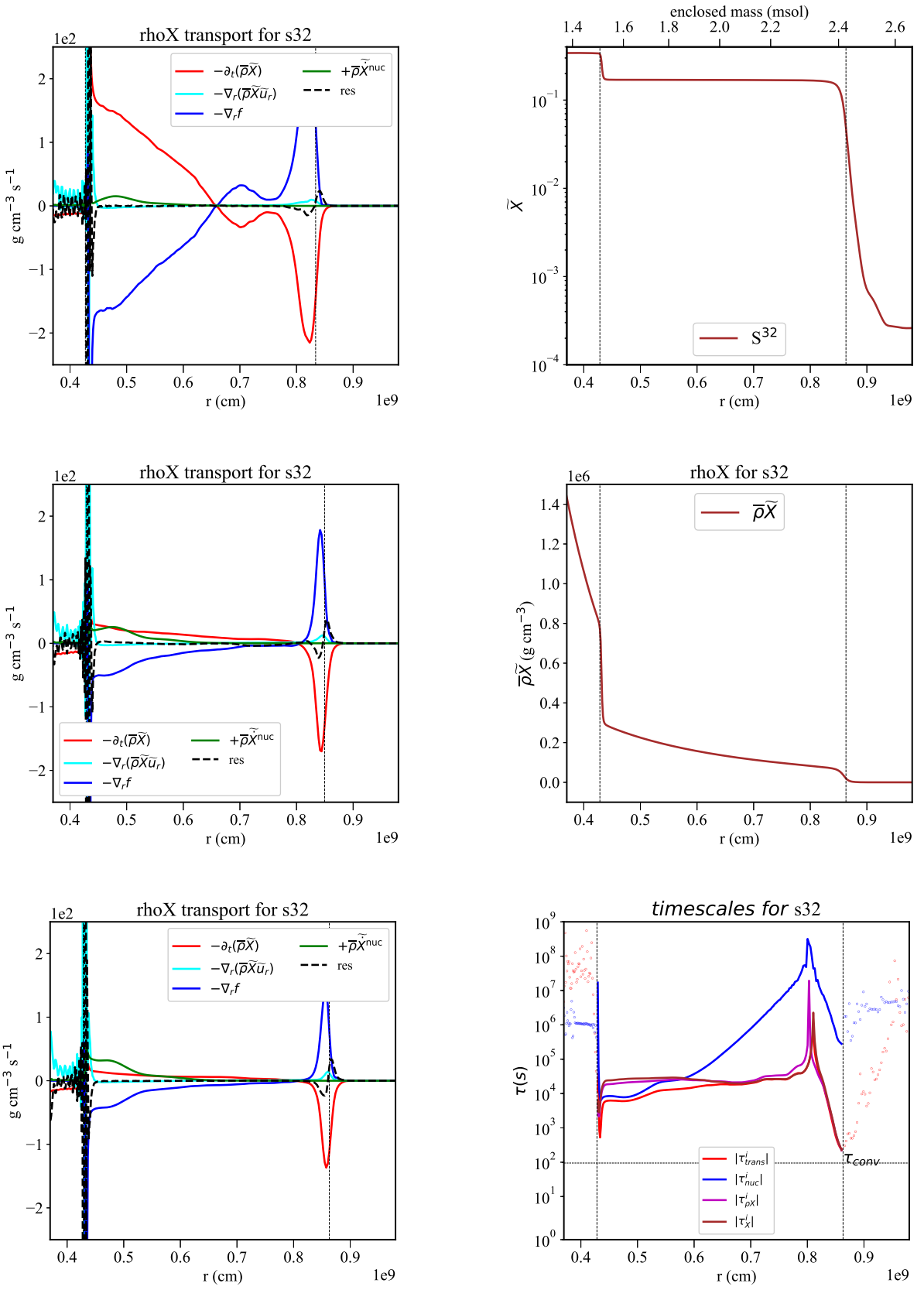

Figure 15. S^{32}: Plot description defined in Fig.5

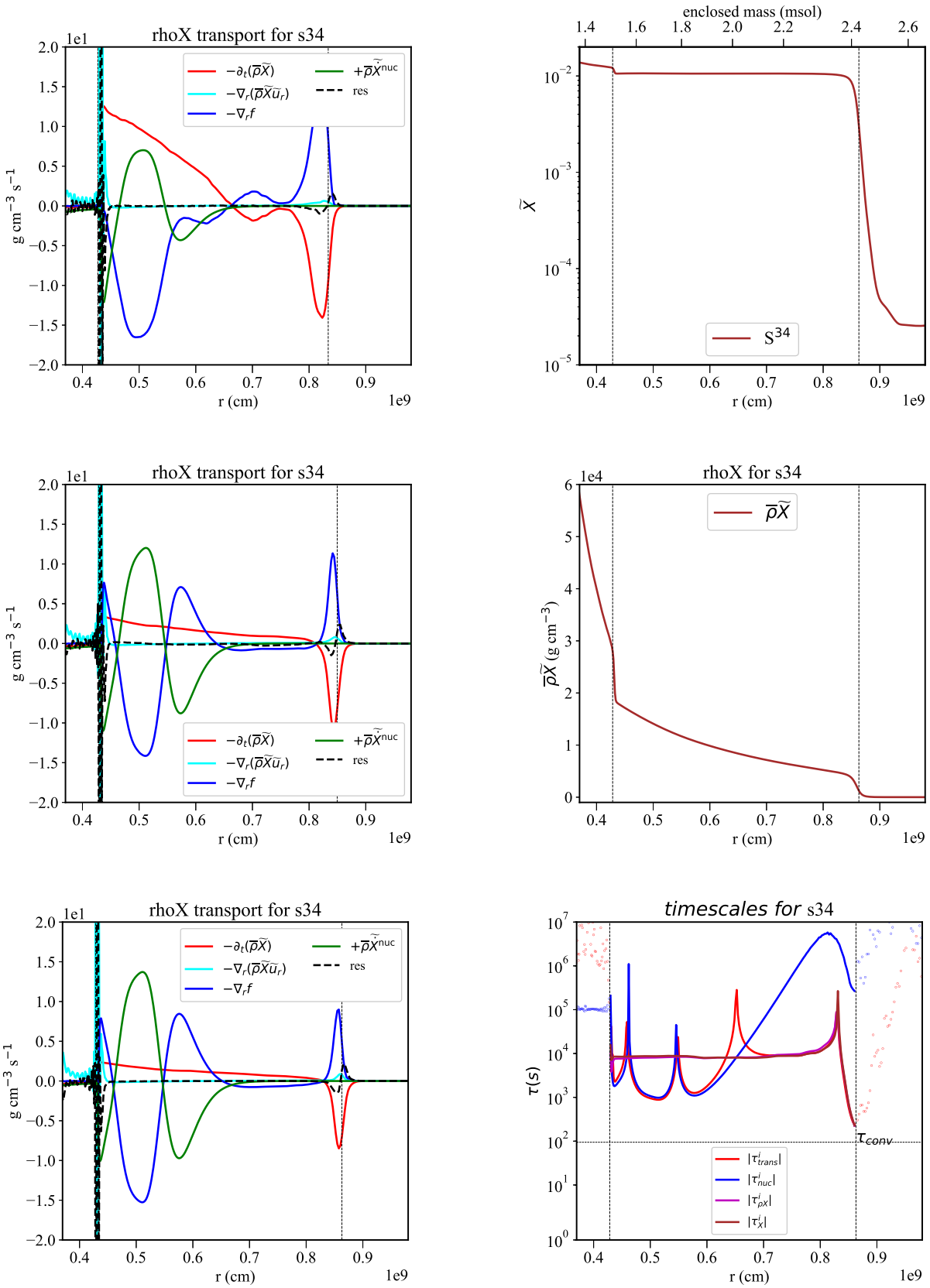

Figure 16. S^{34}: Plot description defined in Fig.5

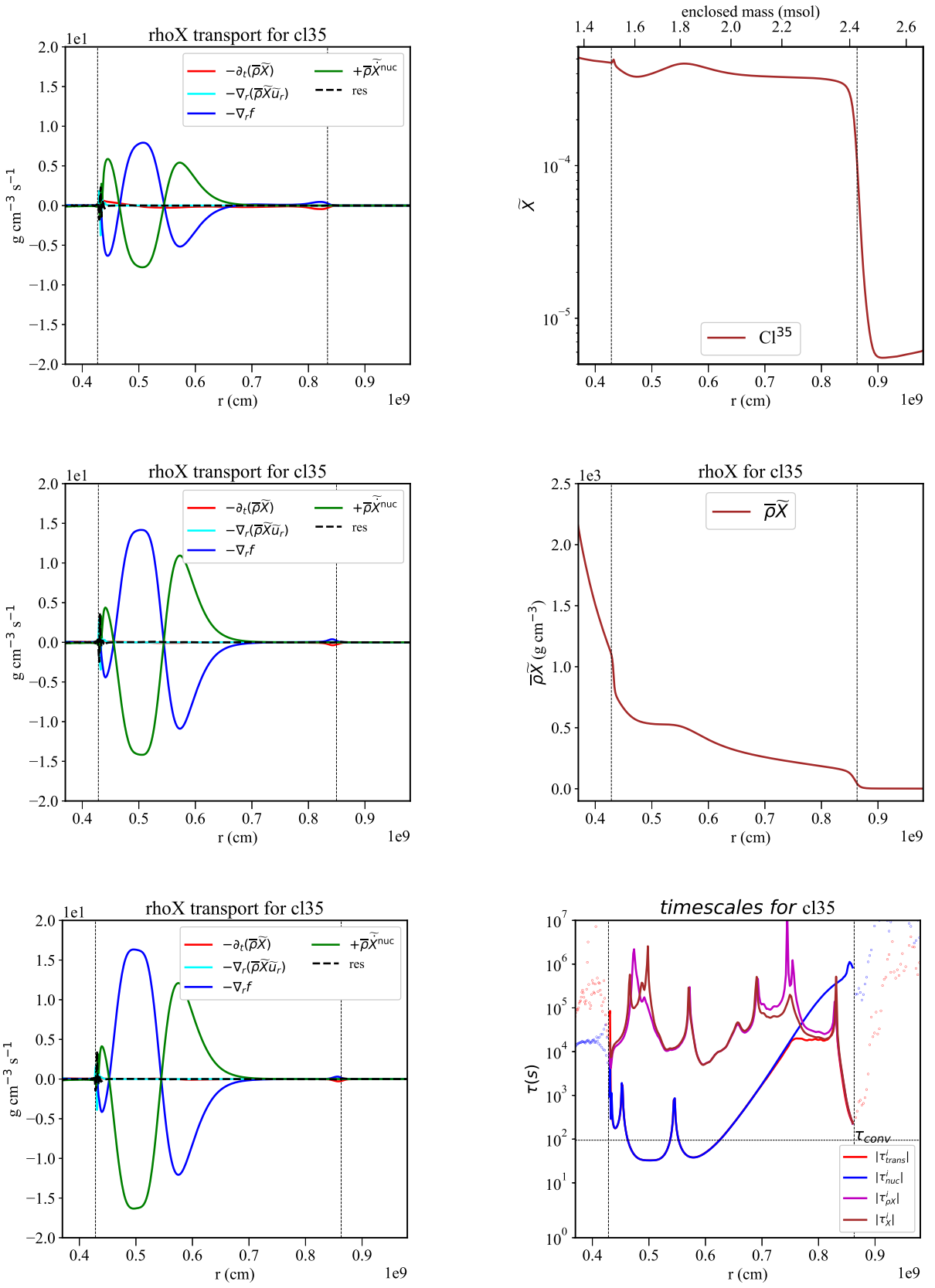

Figure 17. Cl^{35}: Plot description defined in Fig.5

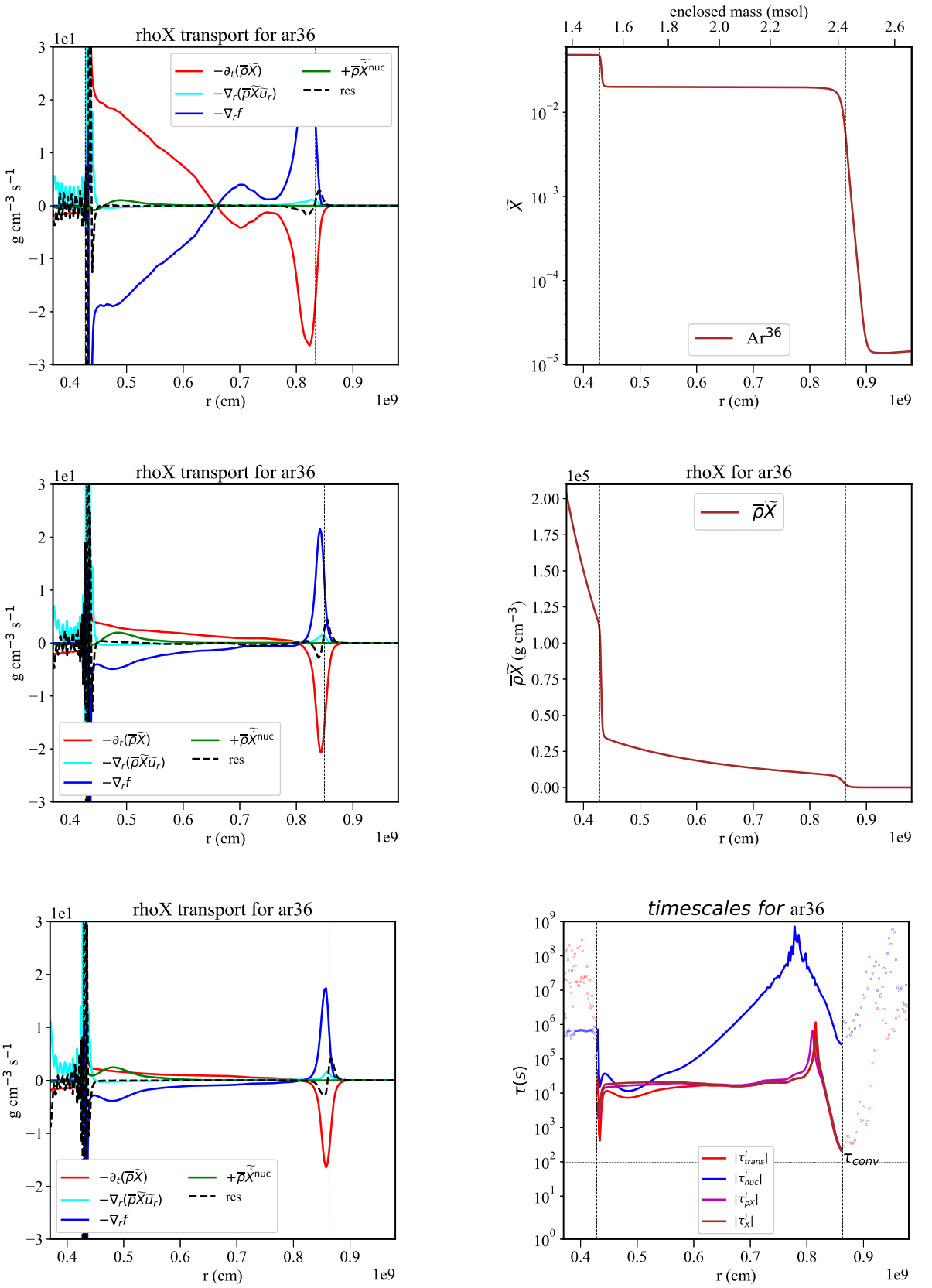

Figure 18. Ar^{36}: Plot description defined in Fig.5

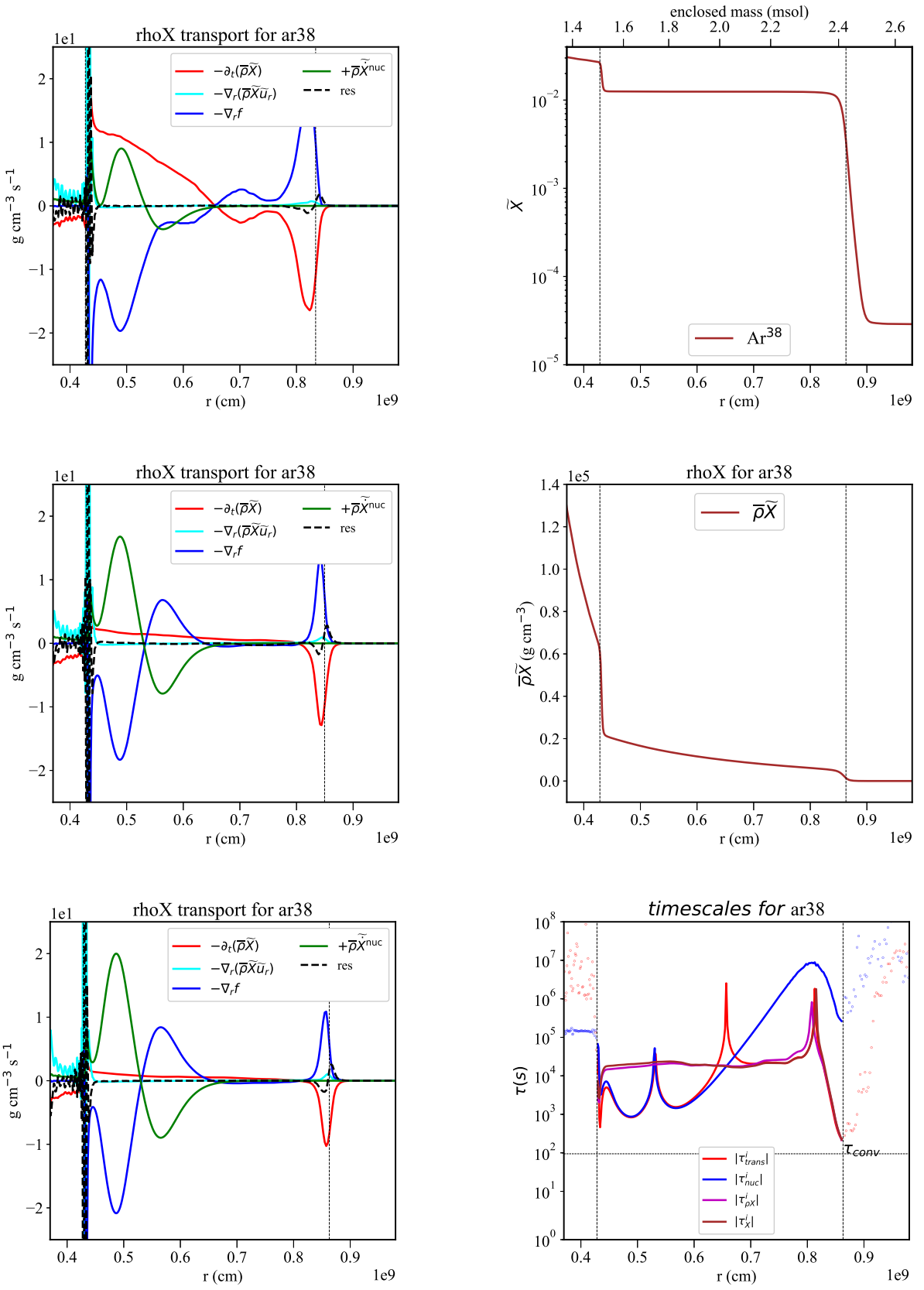

Figure 19. Ar^{38}: Plot description defined in Fig.5

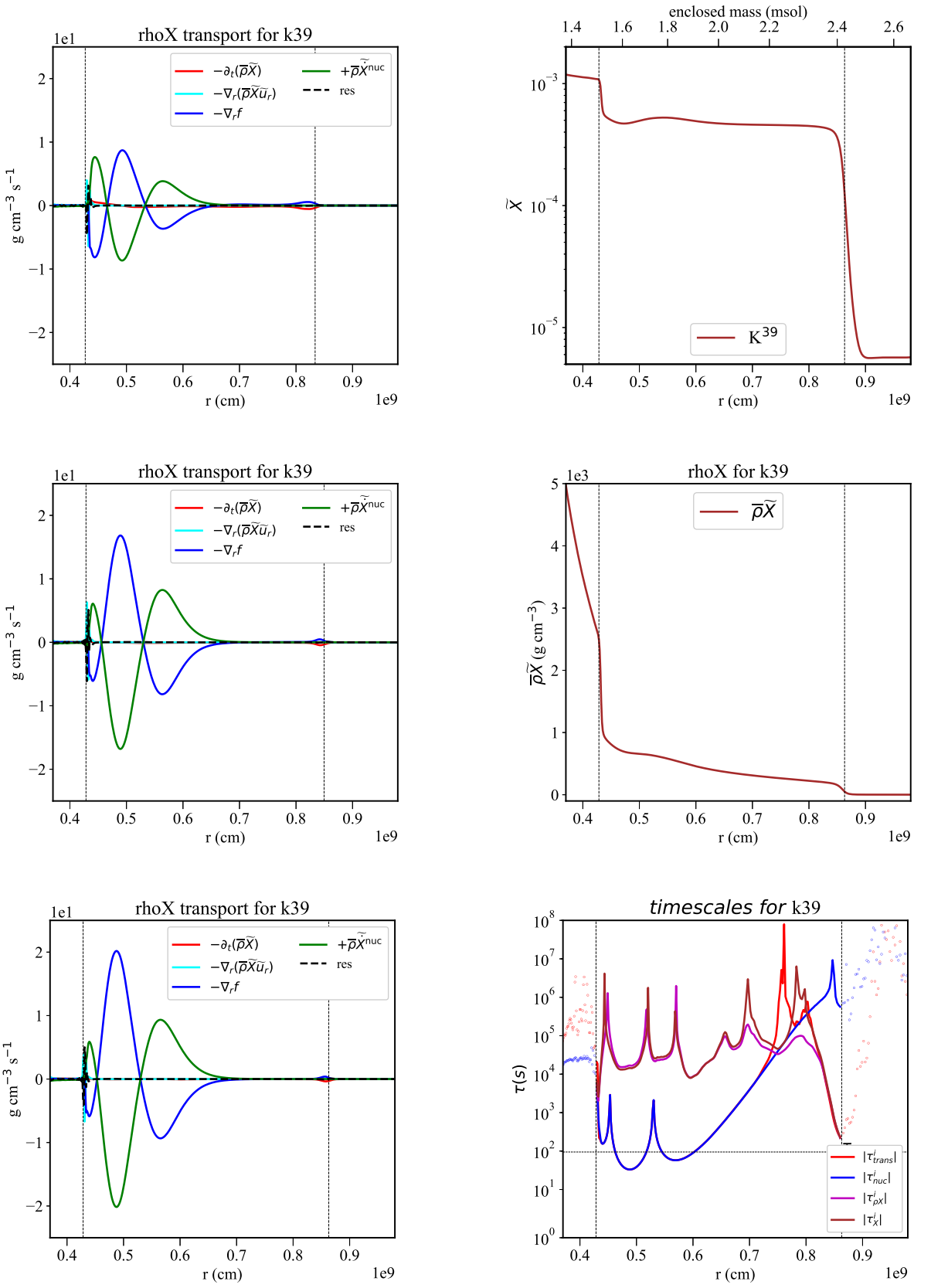

Figure 20. K^{39}: Plot description defined in Fig.5

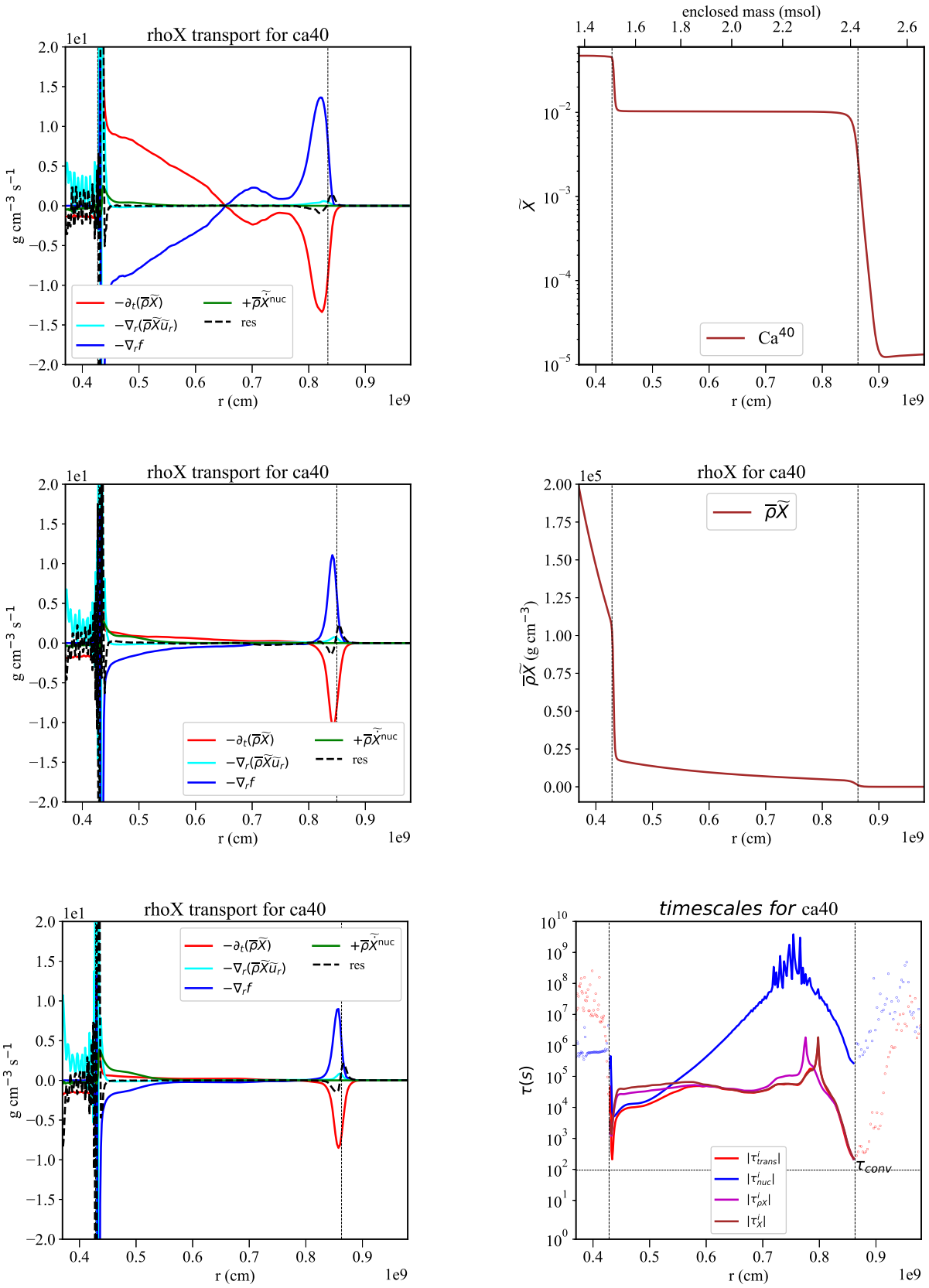

Figure 21. Ca^{40}: Plot description defined in Fig.5

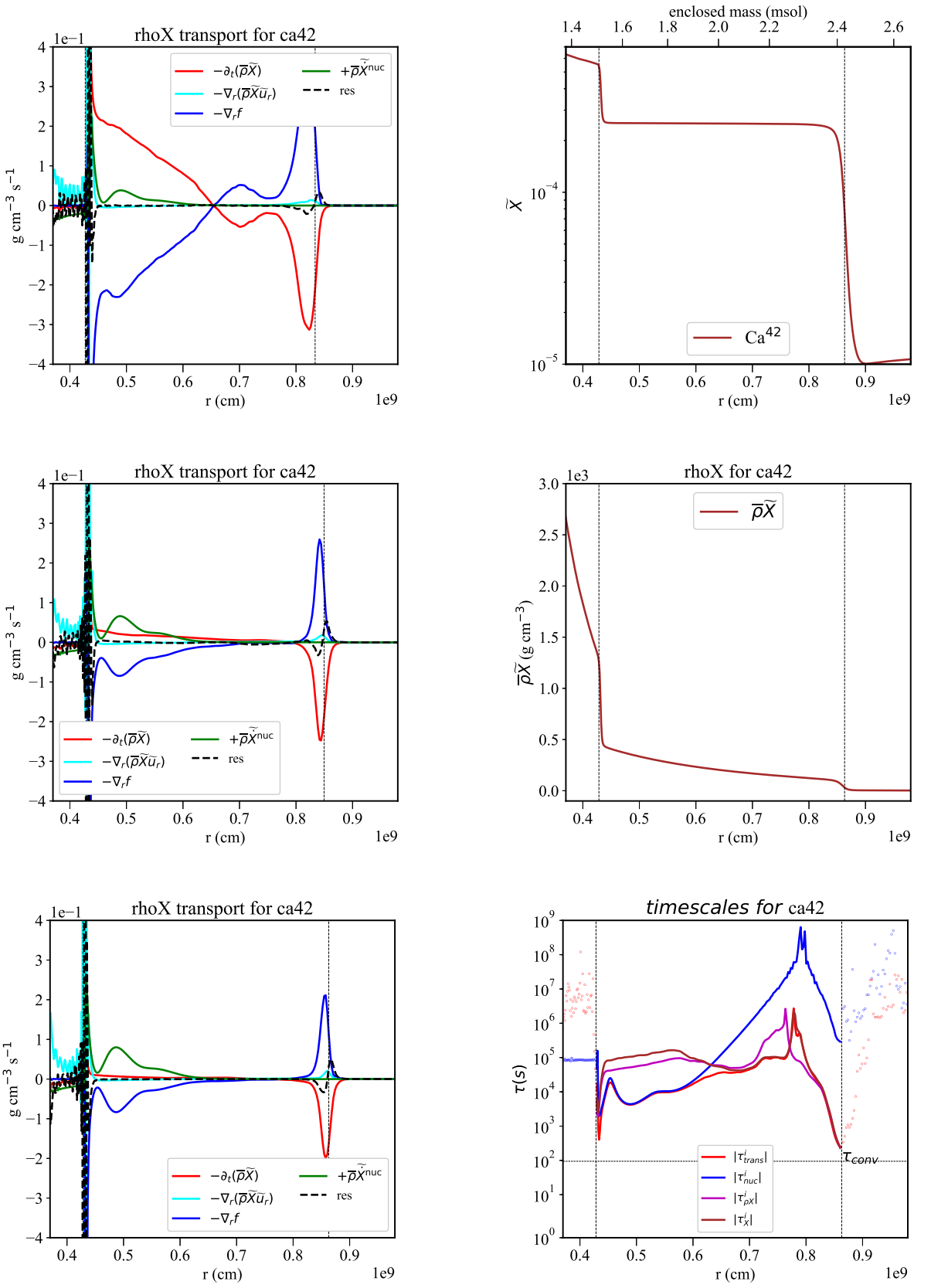

Figure 22. Ca^{42}: Plot description defined in Fig.5

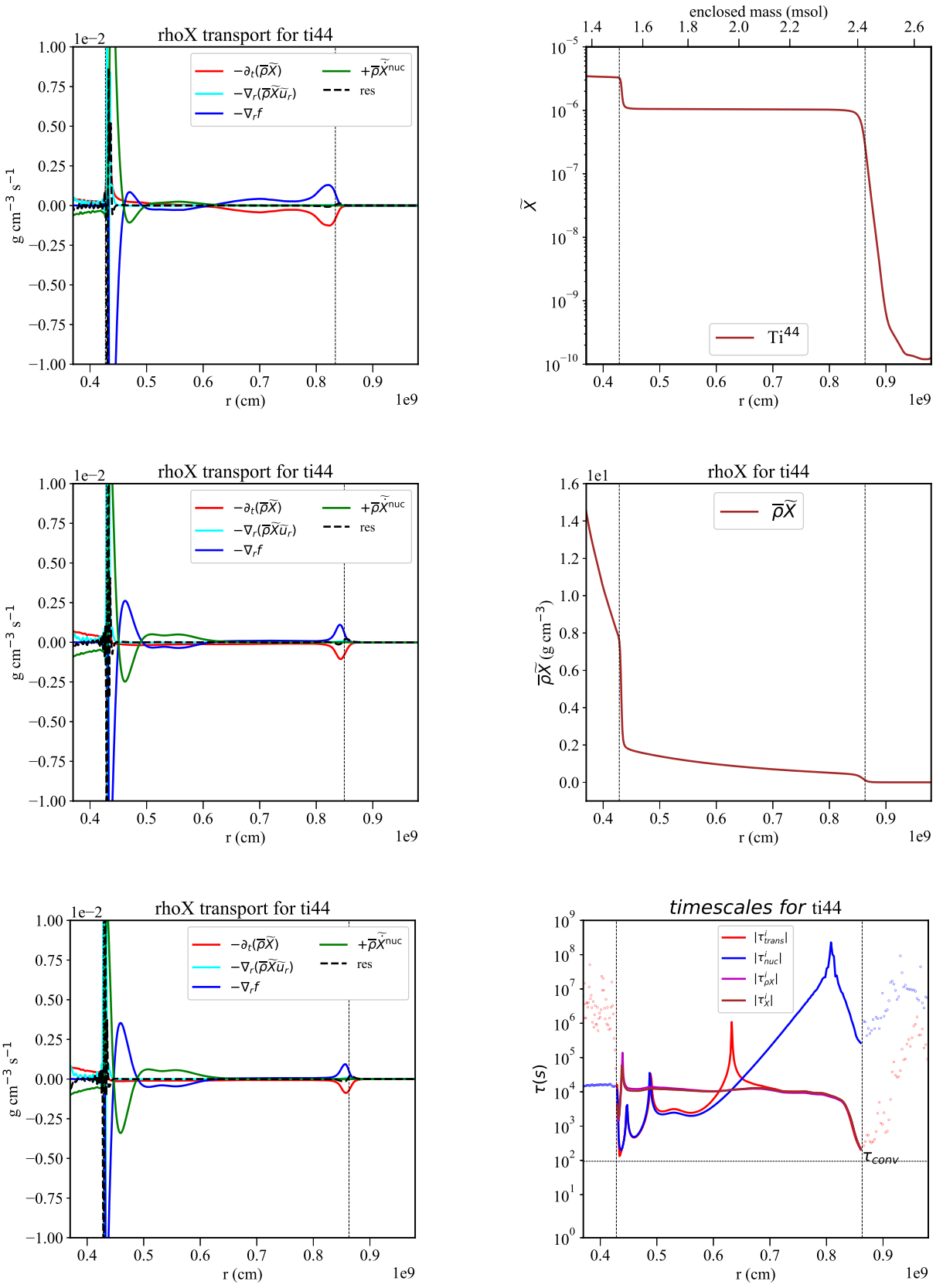

Figure 23. Ti^{44}: Plot description defined in Fig.5

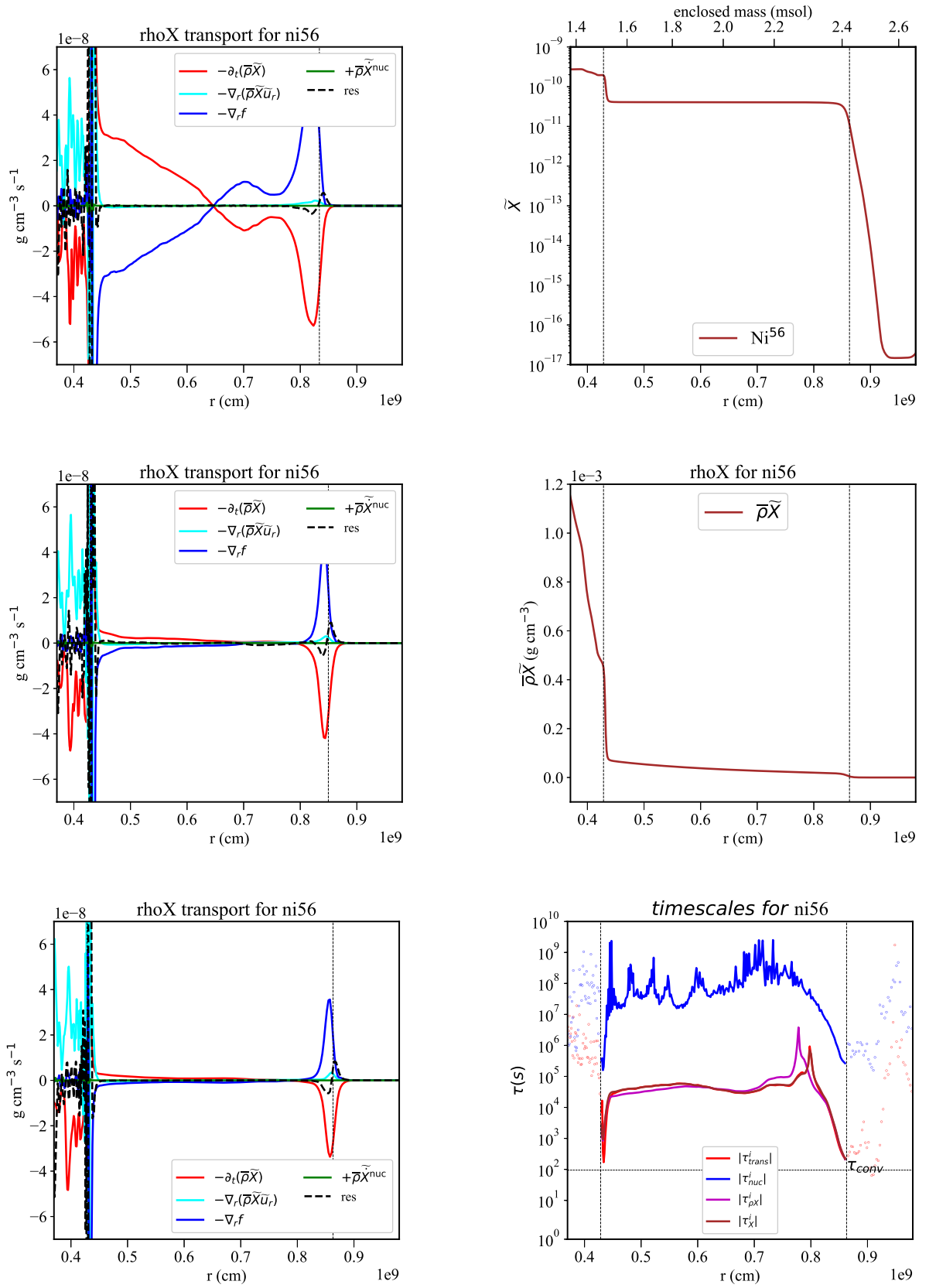

Figure 24. Ni^{56}: Plot description defined in Fig.5

REFERENCES

Mocák M., Meakin C., Viallet M., Arnett D., 2014, arXiv e-prints, p. arXiv:1401.5176

This paper has been typeset from a TEX/LATEX file prepared by the author.